

# Stronger Together: Registering Preoperative Imagery, LUS, and MIS Liver Images

Mohammad Mahdi Kalantari<sup>1</sup>, Erol Ozgur<sup>1</sup>, Mohammad Alkhatib<sup>1</sup>, Navid Rabbani<sup>2</sup>, Yamid Espinel<sup>2</sup>, Richard Modrzejewski<sup>4</sup>, Bertrand Le Roy<sup>3</sup>, Emmanuel Buc<sup>2</sup>, Youcef Mezouar<sup>1</sup>, and Adrien Bartoli<sup>1,2,4</sup>

<sup>1</sup> Clermont Auvergne INP, SIGMA Clermont, Clermont-Ferrand, France.

`mohammad_mahdi.kalantari@sigma-clermont.fr`

<sup>2</sup> University Hospital of Clermont-Ferrand, France.

<sup>3</sup> University Hospital of Saint-Etienne, France.

<sup>4</sup> SurgAR, 22 allée Alan Turing, Clermont-Ferrand, France.

**Abstract.** This study addresses the critical challenges of accurate tumor localization in minimally invasive surgery (MIS) of the liver, where limited visibility and the absence of tactile feedback complicate surgery. The study focuses on integrating all three standard modalities: preoperative 3D models, laparoscopic ultrasound (LUS), and MIS images. Unlike previous approaches, our method exploits the interrelationships among all these modalities, without relying on markers or external sensors, to maximize applicability. It uses an advanced geometric model to integrate the existing registration constraints between pairs of modalities, such as the anatomical landmarks, with new spatial constraints, including the contact of the LUS transducer with the liver and the agreement of the LUS and the preoperative tumor profiles. Experimental validation on phantoms and patient data shows that the method boosts accuracy.

**Keywords:** MIS · Multimodal registration · Tumor localization.

## 1 Introduction

MIS has revolutionized liver surgery but localizing tumors is difficult. In laparoscopic liver resection (LLR), this is mitigated by incorporating two additional modalities beyond MIS images. First, LUS, which is the gold standard, but has multiple drawbacks, including the long learning curve, operator dependence, restricted field of view, and low image quality. Second, preoperative 3D models, reconstructed from preoperative CT or MRI, which are challenging to use due to organ deformation from gas insufflation and mobilization. Augmented reality (AR) has been recently attempted to overcome these challenges [12, 5, 14, 7, 3]. However, the existing methods share the limitation of using only two out of the three typical modalities, resulting in ill-posed registration problems.

We propose to integrate the three modalities in a unified registration, without the need for markers or external sensors, thereby preserving the sterility and

---

Implementation available at: [github.com/MMKalantari/MultiModalLiverReg](https://github.com/MMKalantari/MultiModalLiverReg)

integrity of the operating room (OR) environment. The proposed registration method exploits new prominent constraints between the three pairs of modalities. It concurrently estimates the deformation of the preoperative 3D model and recovers the 6-DoF LUS pose. It outperforms existing methods based on only two modalities, as shown through both qualitative and quantitative results on phantom and patient data.

## 2 Related Work

We review markerless registration methods for all combinations of two modalities and then for the three modalities. In preoperative 3D model to MIS image registration, the early method [21] performed rigid registration, which is generally inaccurate. It was followed by deformable registration methods [14, 12, 5, 10, 4, 2, 9], all guided by anatomical landmark correspondences, leading to improved accuracies. In preoperative 3D model to LUS registration, existing methods use vessels [16, 19] and kinematic priors [18]. However, even disregarding the 39% failure rate reported in the most recent work [19], this type of registration remains unstable owing to liver deformation. In LUS to MIS image registration, existing methods use electromagnetic (EM) tracking [13], magneto-optic tracking [6], or visual markers [17]. Recently, a markerless vision-based method has been proposed [8, 7]. Lastly, two prior studies addressed the registration of all three modalities and bear the closest resemblance to our approach. The method proposed in [15] is learning-based and patient-specific, requiring retraining for each individual case and relying on synthetic rendering. In contrast, our approach is patient-generic and grounded in a principled mathematical model of inter-modality relationships. This model-based formulation enhances interpretability and enables step-wise error monitoring and control. Moreover, our method remains effective even when the tumor is not visible in the LUS images. [22] uses an EM tracker for the LUS probe, manual initialization, and vessel landmarks. However, EM tracking may be impractical due to sterility and adds clutter to the OR. In contrast, the proposed method eliminates manual initialization and uses existing OR devices (the laparoscope and the LUS), ensuring seamless integration.

## 3 Methodology

### 3.1 Modelling and Main Assumptions

We use **Lap**, **Prp**, and **LUS** as shorthands for the three modalities. The primary inputs and outputs of our system are shown in Fig. 1. We assume **LUS** and **Lap** are synchronized, hence a rigid transformation exists between them.

**Lap** is the MIS camera, aka laparoscope. It gives an RGB image and liver annotations (we use the automatic segmentor [10] of the silhouette, the falciform ligament, and the lower ridge). We use the standard pinhole model, whose intrinsic parameters are in the  $3 \times 3$  matrix  $K$  with  $f_x, f_y$  the focal lengths

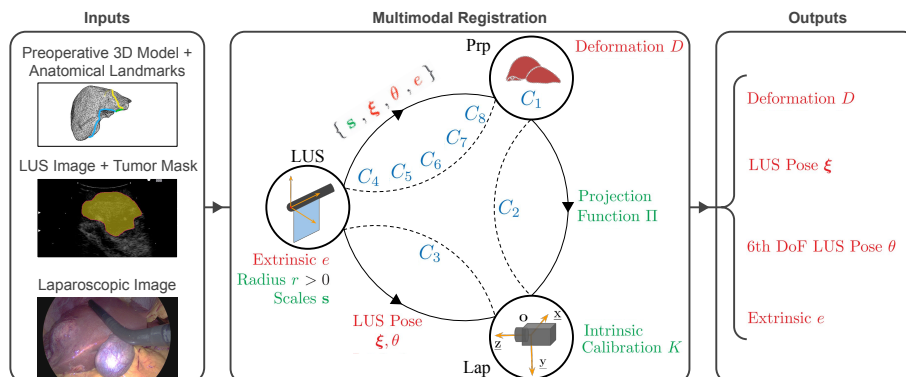


**Fig. 1.** Modalities, parameters, and relationships. Optimizable parameters are in red, fixed ones in green, and cost terms for each pair of modalities (except  $C_1$ ) in blue.

and  $x_0, y_0$  the principal point in pixels. The camera is calibrated, and the image is undistorted using OpenCV. The projection function is thus  $\Pi(X, Y, Z) = (f_x X/Z + x_0, f_y Y/Z + y_0)$ . We define the reference coordinate frame for registration as the standard pinhole coordinate frame with origin at the camera center. *Registration is thus to transform all other entities to the Lap coordinate frame.*

LUS is the laparoscopic ultrasound probe. The image is obtained when the transducer touches the liver. This provides a gray-level image and a binary tumor segmentation mask is generated manually. Following [8, 7], the probe is modeled by a spherocylinder (a cylinder for the head part and a sphere for the tip), with a known radius  $r > 0$ . The probe’s coordinate frame has its origin at the sphere’s center, axis  $Z$  aligned with the cylinder axis and axis  $X$  intersecting with the linear transducer. The probe pose ( $R \in SO_3, T \in \mathbb{R}^3$ ) cannot be estimated from the laparoscopy image only, because of the rotational symmetry of the spherocylindrical probe model about axis  $Z$ , a known issue [8]. Using Euler angles, we thus decompose the pose’s rotation as  $R_X(\alpha)R_Y(\beta)R_Z(\theta)$  and represent the pose in two parts. Part 1 contains the 5 DoF recoverable from the laparoscopy image only,  $\xi = (\alpha, \beta, T)$ . Part 2 contains the 6th DoF, namely  $\theta$ , requiring an extra constraint to be recovered. Finally, the probe has a single extrinsic parameter  $e$  defining the imaging plane offset axis  $Z$ . The intrinsic parameters,  $\mathbf{s} = [s_x, s_y]$ , are pixel-to-mm scales read from the US screen.

Prp is the preoperative image, typically CT or MRI. We assume a preoperative 3D model is reconstructed with MITK as a triangulated mesh with vertices denoted  $D_{\text{Prp}}$  in the preoperative coordinate frame. This comprises the liver surface  $\text{surf}(D_{\text{Prp}})$ , the internal tumors, and the anatomical landmarks (falciform ligament and lower ridge). Registration searches the mesh deformation represented by new vertices  $D$  in the Lap coordinate frame.

### 3.2 Problem Statement and Cost Functions

We use the above modeling to define a minimization problem. The cost function  $C$  has 8 terms  $C_i$  with weights  $\lambda_i > 0$ ,  $i \in [1, 8]$ . The first cost term is a mesh biomechanical deformation energy. All other cost terms capture the modality-pair constraints on registration, the first 3 terms being replicated from the literature and the last 5 being novel. Some terms overlap, as they may be used in initialization or refinement.

**Deformation energy (Prp) [12].** Cost term  $C_1(D)$  maintains the preoperative 3D model's structural integrity during deformation using the neo-Hookean model.

**Anatomical landmarks (Prp-Lap) [10].** Cost term  $C_2(D)$  is the distance between the preoperative 3D model's anatomical landmarks after deformation and projection, and their correspondence in the surgical image.

**Probe reprojection (Lap-LUS) [8].** Cost term  $C_3(\xi) = \sum_{q \in \mathcal{S}} d(q, \Pi(\xi))$  measures the sum of point distances  $d(\cdot, \cdot)$  between each point  $q$  of the observed 2D LUS contour  $\mathcal{S}$  and the reprojection  $\Pi(\xi)$  of the spherocylinder representing the LUS probe to the surgical image.

**Probe contact (Prp-LUS) - non-collision.** Cost term  $C_4(D, \xi)$  prevents probe-liver collision by ensuring the probe remains outside the liver. We sample  $N_{\text{probe}} = 520$  points on the LUS probe stored in  $\mathcal{P}_{\text{probe}}$ . The cost is based on the signed distance  $d_{\pm}(p, \text{surf}(D))$  from a point  $p \in \mathcal{P}_{\text{probe}}$  to the liver surface  $\text{surf}(D)$ . By convention,  $d_{\pm}$  is positive outside the liver. The cost is finally activated at a point  $p$  using the Heaviside function  $H(\cdot)$ , giving:

$$C_4(D, \xi) = \sum_{p \in \mathcal{P}_{\text{probe}}} H(-d_{\pm}(p, \text{surf}(D))). \quad (1)$$

**Probe contact (Prp-LUS) - position.** Cost term  $C_5(D, \xi)$  is the distance between the LUS probe and the liver surface.

$$C_5(D, \xi) = \sum_{p \in \mathcal{P}_{\text{probe}}} d(p, \text{surf}(D)). \quad (2)$$

**Probe contact (Prp-LUS) - orientation.** Cost term  $C_6(D, \xi, \theta)$  is the absolute angle  $\text{ang}(\cdot, \cdot)$  between the LUS probe's imaging plane and the liver surface normals along the transducer. We sample  $N_{\text{trans}} = 32$  points on the LUS transducer stored in  $\mathcal{P}_{\text{trans}}$ . For a point  $p \in \mathcal{P}_{\text{trans}}$ , the cost uses the liver surface normal  $\mathcal{N}(p, \text{surf}(D))$  at the closest point of  $p$ , and the probe orientation  $\mathcal{U}(\xi, \theta)$ , giving:

$$C_6(D, \xi, \theta) = \sum_{p \in \mathcal{P}_{\text{trans}}} \text{ang}(\mathcal{N}(p, \text{surf}(D)), \mathcal{U}(\xi, \theta)). \quad (3)$$

**Tumor profile (Prp-LUS) - shape.** Cost term  $C_7(D, \xi, \theta, e)$  is the distance between the tumor profile from LUS, denoted by  $\mathcal{P}_{\text{prof}}$ , and the slicing  $U(D, \xi, \theta, e)$  of the preoperative 3D model along the LUS imaging plane. We sample  $N_{\text{prof}}$  points from  $U$  with a uniform distance of 1mm, resulting in typically  $N_{\text{prof}} \in$

---

**Algorithm 1: Optimization Criterion**


---

**Inputs:**  $D_{\text{Prp}}$  (*initial liver mesh*),  $\mathbf{s}$  (*LUS scales*),  $I$  (*laparoscopic image*),  
 $K$  (*laparoscope intrinsics*)  
**Outputs:**  $D$  (*deformed liver*),  $\xi$  (*5-DoF LUS pose*),  $\theta$  (*6th DoF LUS pose*),  
 $e$  (*LUS extrinsic*)  
 /\* Initialization \*/  
 1  $D \leftarrow \text{reg\_Prp\_to\_Lap}(D_{\text{Prp}}, I, K)$  // Use [10]  
 2  $\xi \leftarrow \text{estimate\_5DoF\_LUS\_Pose}(I, K)$  // Use [8]  
 3  $D, \xi \leftarrow \arg \min_{D, \xi} C_4(D, \xi) + C_5(D, \xi)$  // Probe-liver contact  
 4  $[\theta, e] \leftarrow [\arg \min_{\theta} C_6(D, \xi, \theta), 0]$  // Transducer-liver contact  
 /\* Refinement \*/  
 5 converged  $\leftarrow$  **False**  
 6 **while** not converged **do**  
     /\* Differential evolution minimization \*/  
 7  $\xi, \theta, e \leftarrow \arg \min_{\xi, \theta, e} C_7(D, \xi, \theta, e) + \lambda_3 C_3(\xi)$   
     /\* Gauss-Newton minimization \*/  
 8  $D^- \leftarrow D$  // Save current deformation  
 9  $D \leftarrow \arg \min_D C_1(D) + \lambda_2 C_2(D) + \lambda_4 C_4(D, \xi) + \lambda_5 C_5(D, \xi) + \lambda_8 C_8(D, \xi, \theta, e)$   
 10 **if**  $\|D - D^-\| < \tau$  **then** converged  $\leftarrow$  **True** // Convergence verification  
 11 **end**

---

[30, 250] points. We construct the transformation matrix  $E$  from the LUS parameters  $\xi, \theta, e$ , which maps the LUS image coordinate frame to the base coordinate frame and assemble the scale matrix  $S = \text{diag}(s_x, s_y)$  from scale vector  $\mathbf{s}$ . Using these, a LUS tumor profile point  $p$  is transformed to the Lap coordinate frame as  $SE^{-1}p$ , giving:

$$C_7(D, \xi, \theta, e) = \frac{1}{N_{\text{prof}}} \sum_{p \in \mathcal{P}_{\text{prof}}} \min_i (d(SE^{-1}(p - \bar{p}), U_i - \bar{u})), \quad (4)$$

where centroids  $\bar{p} = \text{mean}(\mathcal{P})$  and  $\bar{u} = \text{mean}(U)$  are for translation invariance. **Tumor profile (Prp-LUS) - position.** Cost term  $C_8(D, \xi, \theta, e) = \|SE^{-1}\bar{p} - \bar{u}\|$  is the distance between the centroids of the tumor profiles from LUS and Prp.

### 3.3 Minimization Method

The optimization problem involves a large number of unknowns (typically 600 to 800), an 8 cost terms of different nature (smooth or non-continuously differentiable, most of them non-convex), proscribing random initialization. We propose an initialization and refinement method in algorithm 1.

**Initialization.** Structured initialization exploits variable dependencies and existing solution methods. It starts with [10] which finds initial deformation parameters  $D$ , and follows with [8] which finds an initial LUS 5-DoF pose  $\xi$ . A first level of LUS to Prp constraint is then introduced through  $C_4$  and  $C_5$ , ensuring proper contact between the LUS probe and the liver surface by updating

	# Phantom								
	1	2	3	4	5	6	7	8	Avg
Base Method [10]	37.68	23.44	23.46	17.01	20.92	21.08	20.52	23.64	23.47
Base + Contact	-26%	-3%	-6%	+23%	+9%	+3%	-18%	-15%	-4%
Base + All	-49%	-72%	-36%	-55%	-35%	-48%	-24%	-22%	-43%

**Table 1.** TRE (mm) for the base method in the phantom study, with percentage changes from contact-only and all proposed constraints.

$D$  and  $\xi$ . Finally, the missing LUS parameters are initialized while accounting for all optimization variables. Specifically, the missing LUS pose rotation angle  $\theta$  is initialized using the liver surface normals, while the extrinsic offset  $e$  is set to zero, initializing the transducer close to the probe tip.

**Refinement.** We split the minimization into two parts. First, we consider the non-smooth terms  $C_3$  and  $C_7$ , which we optimize by means of differential evolution. Second, we consider the smooth terms –all the others– which we optimize by Gauss-Newton. Both steps use the SciPy library. We accelerate and stabilize the process using dimensionality reduction [12], reducing the mesh vertices to 200, and an explicit coding of the Jacobian matrix function. Convergence occurs when the deformation parameters change under a threshold  $\tau$ .

## 4 Experimental Results and Discussion

We used constant hyperparameters, empirically set at  $\lambda_2 = 0.1$ ,  $\lambda_3 = \lambda_4 = \lambda_5 = 10$ ,  $\lambda_8 = 3$ , and  $\tau = 3.5$ .

### 4.1 Phantom Study

This study simulates 8 deformations to a 3D liver model with a virtual tumor following [20, 1]. The deformed models are 3D printed, with known GT tumor position, and anatomical landmarks. An instance of the experiment setup is brought in Fig. 2a. We use a real LUS probe and simulate the LUS image. We first estimate the LUS pose using an Aruco marker. The imaging plane is then intersected with the GT tumor, and Gaussian noise is added to the resulting contour points. Then the anatomical landmarks in the laparoscope image are annotated manually, and the rest of the experiment follows algorithm 1. The simulated LUS detects the tumor in the deformed model (and not the GT tumor). The results are shown in Table 1. The mean absolute error (MAE) for the pose angle  $\theta$  is  $10.3^\circ$  with  $6.3^\circ$  StDev, and for the extrinsic parameter  $e$  it is 1.2mm with 0.4mm StDev. The benefit in terms of tumor Target Registration Error (TRE) of co-registering the 3 modalities in our method is striking, with an average reduction of 43% compared to existing work.

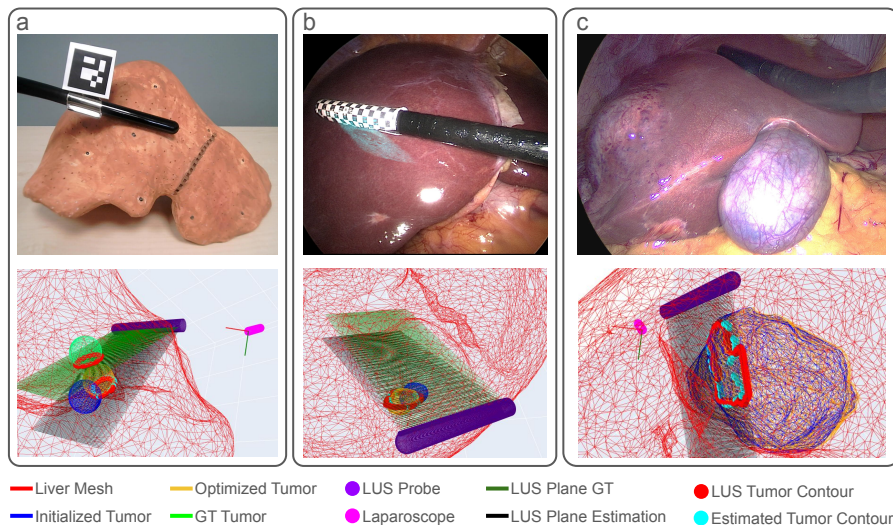


**Fig. 2.** Experiments: (a) phantom, (b) public benchmark, (c) patients qualitative.

## 4.2 Public Benchmark

We use the public dataset [17], which allows for a direct comparison of the TRE between methods and provides ground truth for the LUS imaging plane obtained using markers on the probe (these markers are not used by our method). Fig. 2b demonstrates an instance of the experiment. Table 2 shows results for 3 patients. The proposed method slightly outperforms the best result [2] for P1 (from 8.25mm to 7.76mm), substantially outperforms the best result [12] for P3 (from 17.60mm to 8.58mm), and underperforms the best result [10] for P4 (from 7.23mm to 12.35mm). As observed, our method outperforms the existing approaches when the tumor on the surgery day closely resembles the preoperative model, as can be seen on average without P4 that the error from the best result [9]

	Tumor TRE (mm)							Tumor evolution
	MA	M1	M2	M3	LMR	NM	Ours	
P1	15.14	8.25	9.49	14.87	17.40	14.82	<b>7.76</b>	No
P3	30.48	28.40	25.04	22.40	17.60	20.15	<b>8.58</b>	No
P4	16.29	15.83	18.35	<b>7.23</b>	17.00	12.95	12.35	<b>Yes</b>
Avg. w/o P4	22.81	18.33	17.27	18.64	17.50	17.49	<b>8.17</b>	No
Avg.	20.63	17.49	17.63	14.83	17.33	15.97	<b>9.56</b>	<b>Mixed</b>

**Table 2.** Tumor TRE on public benchmark [17]. ‘Tumor evolution’ indicates a change in tumor size between preoperative imaging and surgery. MA is manual rigid registration, M1 is [2], M2 is [9], M3 is [10], LMR is [12], and NM is [14].

is reduced by 53%, from 17.27mm to 8.17mm by our method. It also continues to function effectively even when there is tumor growth between the preoperative imaging and the surgery day, though the performance may be affected in such cases. The average MAE estimation for  $\theta$  is  $8.7^\circ$  with  $4.7^\circ$  StDev.

### 4.3 Qualitative Study

We conducted a qualitative study on two additional patients with 5 images, illustrated in Fig. 2c, with 4 validation steps. *(i)* The 5-DoF LUS pose  $\xi$  was validated by comparing the silhouette of the reprojected LUS probe model to **Lap**, using the optimized pose parameters, with the segmented LUS probe. The average IoU in the experiments was 97%. *(ii)* The 6th DoF LUS pose  $\theta$  was evaluated by uniformly sampling values in  $[0, 2\pi)$  by steps of  $0.1^\circ$ . For each value, we compared the LUS image tumor with the tumor cross-section obtained from **Prp**. The estimated  $\theta$  always obtained the least distance, with an average of 1.2mm, indicating its optimality. *(iii)* Liver deformation was evaluated using the distance between the anatomical landmarks reprojected from the optimized model and their observation in **Lap**; the average distance was  $31 \pm 6$  pixels, which is reasonable given the large HD image resolution. *(iv)* The tumor shape and translation were evaluated before and after optimization. If the tumor or surrounding tissue exhibited significant deformation, *i.e.* changing the volume more than 20%, it indicated inconsistencies in the optimization process. Likewise, if the translation was insufficient to align the tumor with the desired contour, it suggested suboptimal initialization, leading the algorithm to enforce local adjustments constrained by other optimization parameters. In the experiments, neither a significant tumor deformation nor an insufficient translation was observed.

### 4.4 Discussion

Validating registration in surgery is highly challenging. Our approach has been tested retrospectively on 6 patients and 8 phantoms. Qualitative results from 2 patients, along with qualitative and quantitative results for the 8 phantoms and Patients P1 and P3 of [17] highlight the benefits brought by using all 3 standard modalities together. In Section 4.2, Patient P4 highlights the method’s dependency on the similarity between the preoperative tumor model and the actual tumor on the surgery day. If the preoperative model deviates significantly from intraoperative reality, the method remains functional but introduces some errors. That said, it is a natural requirement: *if a mismatch exists between the preoperative and intraoperative models, an augmented reality method should actually not be used at all*. In addition, Patient P2, excluded from Table 2, highlights the base deformation model’s importance. If the base model [10] fails to converge during initialization, subsequent optimization becomes infeasible.

The optimization algorithm runs in  $4 \pm 1$  minutes on an average laptop. With automated intraoperative image annotation [11] and manual tumor annotation in the LUS image, the entire process completes in under 6 minutes, demonstrating its clinical feasibility for single-shot augmented reality prior to resectioning.

## 5 Conclusion and Future Work

This study presents a novel approach to tumor localization in minimally invasive liver surgery by leveraging the interrelationships among laparoscopic imaging, laparoscopic ultrasound, and preoperative models without requiring additional markers or external sensors. Experimental validation on real patient data, in addition to phantom studies, highlights the method’s superiority over state-of-the-art techniques, achieving high precision while maintaining an acceptable runtime. These results, combined with positive feedback from surgeons regarding workflow integration, demonstrate the potential of this approach to advance tumor localization in liver minimally invasive surgical procedures.

As future work, three directions are proposed. First, automating tumor segmentation in LUS images by means of a neural network. Second, developing a real-time tumor tracking pipeline would leverage the proposed method as an initialization and allow continuous tumor tracking during surgery. Third, exploiting the proposed method in other MIS procedures.

**Acknowledgments.** This work is funded by project ANR JCJC - IMMORTALLS.

**Disclosure of Interests.** The authors declare no competing interests for this article.

## Bibliography

- [1] [https://encov.ip.uca.fr/ab/code\\_and\\_datasets/](https://encov.ip.uca.fr/ab/code_and_datasets/)
- [2] Adagolodjo, Y., Trivisonne, R., Haouchine, N., Cotin, S., Courtecuisse, H.: Silhouette-based pose estimation for deformable organs application to surgical augmented reality. pp. 539–544 (Sept 2017)
- [3] Ali, S., Espinel, Y., Jin, Y., Liu, P., Güttner, B., Zhang, X., Zhang, L., Dowrick, T., Clarkson, M.J., Xiao, S., Wu, Y., Yang, Y., Zhu, L., Sun, D., Li, L., Pfeiffer, M., Farid, S., Maier-Hein, L., Buc, E., Bartoli, A.: An objective comparison of methods for augmented reality in laparoscopic liver resection by preoperative-to-intraoperative image fusion from the miccai2022 challenge. *Medical Image Analysis* **99**, 103371 (2025)
- [4] Espinel, Y., Özgür, E., Calvet, L., Le Roy, B., Buc, E., Bartoli, A.: Combining visual cues with interactions for 3D-2D registration in liver laparoscopy. *Ann. Biomed. Eng.* **48**(6), 1712–1727 (Jun 2020)
- [5] Espinel, Y., Rabbani, N., Bui, T.B., Ribeiro, M., Buc, E., Bartoli, A.: Keyhole-aware laparoscopic augmented reality. *Medical Image Analysis* **94**, 103161 (2024). <https://doi.org/10.1016/j.media.2024.103161>
- [6] Feuerstein, M., Reichl, T., Vogel, J., Schneider, A., Feussner, H., Navab, N.: Magneto-optic tracking of a flexible laparoscopic ultrasound transducer for laparoscope augmentation. In: *Medical Image Computing and Computer-Assisted Intervention – MICCAI 2007*, pp. 458–466. Springer Berlin Heidelberg, Berlin, Heidelberg (2007)
- [7] Kalantari, M.M., Ozgur, E., Alkhatib, M., Buc, E., Le Roy, B., Modrzejewski, R., Mezouar, Y., Bartoli, A.: LARLUS: laparoscopic augmented reality from laparoscopic ultrasound. *Int. J. Comput. Assist. Radiol. Surg.* **19**(7), 1285–1290 (Jul 2024). <https://doi.org/10.1007/s11548-024-03134-x>
- [8] Kalantari, M.M., Ozgur, E., Alkhatib, M., Buc, E., Le Roy, B., Modrzejewski, R., Mezouar, Y., Bartoli, A.: Markerless ultrasound probe pose estimation in mini-invasive surgery. *IEEE International Conference on Robotics and Automation, ICRA* (2024)
- [9] Koo, B., Ozgur, E., Roy, B.L., Buc, E., Bartoli, A.: Deformable registration of a preoperative 3d liver volume to a laparoscopy image using contour and shading cues. In: *International Conference on Medical Image Computing and Computer-Assisted Intervention* (2017)
- [10] Labrunie, M., Ribeiro, M., Mourtheadhoi, F., Tilmant, C., Le Roy, B., Buc, E., Bartoli, A.: Automatic preoperative 3d model registration in laparoscopic liver resection. *IJCARS* **17**(8), 1429–1436 (Aug 2022)
- [11] Labrunie, M.: Contributions to the Automation of Preoperative 3D Model to 2D Image Registration in Mini-Invasive Liver Surgery. Ph.D. thesis, Université Clermont Auvergne (2024)
- [12] Labrunie, M., Pizarro, D., Tilmant, C., Bartoli, A.: Automatic 3d/2d deformable registration in minimally invasive liver resection using a mesh recovery network. In: *Medical Imaging with Deep Learning. Proceedings of*

- Machine Learning Research, vol. 227, pp. 1104–1123. PMLR, PMLR (10–12 Jul 2024)
- [13] Liu, X., Plishker, W., Shekhar, R.: Hybrid electromagnetic-ArUco tracking of laparoscopic ultrasound transducer in laparoscopic video. *Journal of Medical Imaging* **8**(01) (Feb 2021). <https://doi.org/10.1117/1.jmi.8.1.015001>
  - [14] Mhiri, I., Pizarro, D., Bartoli, A.: Neural patient-specific 3D-2D registration in laparoscopic liver resection. *IJCARS* (Jul 2024)
  - [15] Montaña-Brown, N., Ramalhinho, J., Koo, B., Allam, M., Davidson, B., Gurusamy, K., Hu, Y., Clarkson, M.J.: Towards multi-modal self-supervised video and ultrasound pose estimation for laparoscopic liver surgery. In: *Simplifying Medical Ultrasound*. pp. 183–192. Springer International Publishing, Cham (2022)
  - [16] Montaña-Brown, N., Ramalhinho, J., Allam, M., Davidson, B., Hu, Y., Clarkson, M.J.: Vessel segmentation for automatic registration of untracked laparoscopic ultrasound to ct of the liver. *International Journal of Computer Assisted Radiology and Surgery* (May 2021)
  - [17] Rabbani, N., Calvet, L., Espinel, Y., Roy, B.L., Ribeiro, M., Buc, E., Bartoli, A.: A methodology and clinical dataset with ground-truth to evaluate registration accuracy quantitatively in computer-assisted laparoscopic liver resection. *Computer Methods in Biomechanics and Biomedical Engineering: Imaging & Visualization* **10**(4), 441–450 (2022)
  - [18] Ramalhinho, J., Tregidgo, H., Allam, M., Travlou, N., Gurusamy, K., Davidson, B., Hawkes, D., Barratt, D., Clarkson, M.J.: Registration of untracked 2d laparoscopic ultrasound liver images to ct using content-based retrieval and kinematic priors. In: Wang, Q., Gomez, A., Hutter, J., McLeod, K., Zimmer, V., Zettinig, O., Licandro, R., Robinson, E., Christiaens, D., Turk, E.A., Melbourne, A. (eds.) *Smart Ultrasound Imaging and Perinatal, Preterm and Paediatric Image Analysis*. pp. 11–19. Springer International Publishing, Cham (2019). [https://doi.org/10.1007/978-3-030-32875-7\\_2](https://doi.org/10.1007/978-3-030-32875-7_2)
  - [19] Ramalhinho, J., Koo, B., Montaña-Brown, N., Saeed, S.U., Bonmati, E., Gurusamy, K., Pereira, S.P., Davidson, B., Hu, Y., Clarkson, M.J.: Deep hashing for global registration of untracked 2d laparoscopic ultrasound to ct. *International Journal of Computer Assisted Radiology and Surgery* **17**(8), 1461–1468 (Apr 2022). <https://doi.org/10.1007/s11548-022-02605-3>
  - [20] Ribeiro, M., Espinel, Y., Rabbani, N., Pereira, B., Bartoli, A., Buc, E.: Augmented reality guided laparoscopic liver resection: A phantom study with intraparenchymal tumors. *J. Surg. Res.* **296**, 612–620 (Apr 2024)
  - [21] Robu, M.R., Ramalhinho, J., Thompson, S., Gurusamy, K., Davidson, B., Hawkes, D., Stoyanov, D., Clarkson, M.J.: Global rigid registration of CT to video in laparoscopic liver surgery. *Int. J. Comput. Assist. Radiol. Surg.* **13**(6), 947–956 (Jun 2018)
  - [22] Song, Y., Totz, J., Thompson, S., Johnsen, S., Barratt, D., Schneider, C., Gurusamy, K., Davidson, B., Ourselin, S., Hawkes, D., Clarkson, M.J.: Locally rigid, vessel-based registration for laparoscopic liver surgery. *International Journal of Computer Assisted Radiology and Surgery* **10**(12), 1951–1961 (Jun 2015)